3 Cobalt Supported Ψ-Graphene: A Proficient SAC for CO Oxidation Reaction

In this chapter, we discuss our work on investigating the catalytic behavior of Co SACs supported over recently predicted Ψ-graphene substrate (Co@PG) towards poisoning-free CO oxidation process, which is the reaction between CO and O_2 molecule to form CO_2. We discussed the stability of Co@PG at various anchoring locations in terms of binding energy and Co-atom diffusion over the substrate. Furthermore, we investigated the adsorption of reactants on Co@PG correlated it with d-band properties of Co@PG and used it as a screening criteria for selecting reaction mechanism. We discussed reduced CO poisoning effect of Co@PG, which is attributed to its lesser affinity for CO than O_2. Using the CI-NEB approach, we calculated the activation energy (E_a) and minimal energy path of the complete CO oxidation reaction over Co@PG via Langmuir-Hinshelwood (LH) and Eley-Rideal (ER). With E_a values of 0.19 eV and 0.27 eV for the 1^{st} and 2^{nd} half reactions of CO oxidation, respectively, Co@PG is thus found to be a practicable, non-noble transition metal SACs for CO oxidation reaction preferring ER mechanism.

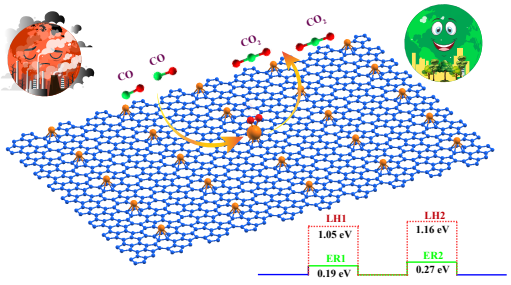

FIGURE 3.1: Graphical Abstract

3.1 Introduction

The ever-escalating environmental pollution and ultimately the increment in the global warming, attributed to the raising concentration of the exhaust gases (CO_x, NO_x, CH_x) in atmosphere due to major contribution from the incomplete combustion of fossil fuels or petroleum products in industrial processes and automobiles[1–3]. The conversion of these exhaust gases into a relatively benign gases is a crucial societal issue at the global level to be solve. It is the only way to reduce/control the amount of concentration of these gases into the environment and fuel cell poisoning[4]. CO oxidation by molecular oxygen (O_2) has garnered heightened attention not only because it leads to a relatively less detrimental carbon dioxide (CO_2) gas but also because it serves as a fundamental benchmark reaction for assessing the catalyst effectivity and efficiency[5, 6].This dual significance has catapulted CO oxidation reaction into the spotlight in the realm of heterogeneous catalysis.

From decades, traditionally existing catalysts, especially of some noble metals such as Au[7, 8], Pt[9–11], Pd[12–14] are known to display exemplary catalytic activity towards CO oxidation reaction. Given their high cost, high operational temperature, exiguity and CO poisoning effect are hampering their usage in commercial applications[15]. Therefore, complete elimination of these metals in scheming a rational catalyst for catalytic CO oxidation is yet an arduous task for the researchers. The improvement in efficiency and preservation of their catalytic activity could be possible with formation of bimetallic catalysts with low cost transition metals like Fe[16], Cu[17], Ni[18] and reducing the size of catalysts to nanoclusters or even smaller which is the key to proceed in this respect. The approach of downsizing of the particle to atomic scale, leads to amplification in cayalytic activity due to their partially filled d-states and introduction of the quantum confinement[19–22]. In this regard, designing a catalyst wherein the atomically dispersed single atoms act as an active site anchored by some substrates is known as 'single atom catalysts' (SAC). The field of SACs left open by Qiao et al. after they designed first practical Pt_1/FeO_x SAC which exhibited exceptional catalytic performance for CO oxidation reaction[23]. Since then, numerous SACs primarily comprising of noble metals like Pt[24], Pd[25], Ni[26, 27], Cu[28], Ir[29], Fe[30], Au[31] and Ag[32–35], have been extensively studied for CO oxidation reaction and various other important reactions. For instance, Rao et al. proposed Pt/Pd@CN monolayer as a promising catalyst for CO oxidation, with energy barrier of 0.68 eV

(Pt@CN) via LH Mechanism and 0.48 eV (Pd@CN) via termolecular Eley-Rideal (TER) mechanism[36]. Liu et al. reported the improved catalytic properties of Pd is attributed to the Pd-C interaction in Pd@graphene SAC[12]. Karmakar et al. investigated the CO oxidation reaction of GeS monolayer supported noble- metal (Pd, Pt, Rh, Ir, Ag, Au) SAC[37].

In order to design a stable and active SACs, it is of utmost importance to get the profound knowledge of the origin of peerless catalytic properties. Apart from being utilized 100% as an metal active site[38], it has been found that the strong metal-support interaction not only offers stability to a SAC by immobilizing the dispersed atom but also alter its electronic states thereby changing its intrinsic behaviour and enhancing it's activity as a catalyst[39, 40]. As always for SACs, carbon based support like graphene, defective graphene, graphtic carbon-nitrides (CN, g-C_3N_4) and graphdiyne are dominating this field as they are highly stable under ambient reaction condition and can be easily synthesize. The tunable morphologies, ordered porosity and proficiency to fixate dispersed metal-atoms are the key factors of carbon-based materials as supports to SACs[41, 42].

The Ψ-graphene (PG), a two-dimensional metallic allotrope of graphene, consists of 12 carbon atoms per unit cell was introduced in 2017 by Li et al[43]. They provided the opportunity in exploiting this new alternative material as support of SACs and ultimately to study its ability towards uniform dispersivity and stable anchoring site of metals atoms. This investigation would be desirable to develop insight into a rational design of catalyst.

In search of economically competent catalyst by eliminating the usage of noble metals, we systematically investigated the catalytic performance of cobalt (Co) single-atom catalyst supported over Ψ-graphene (Co@PG) using density functional theory (DFT) calculations. The stability of PG was investigated by the phonon calculations along with the ab initio molecular dynamics (AIMD) calculations which confirm that the PG is both dynamically and thermally stable at room temperature and also at higher temperature up to 1000K[43]. In this study, we aim to provide theoretical insights on the stability, activity and durability of Co@PG for the CO oxidation reaction via computing and analysing the structural, electronic and catalytic properties of proposed SACs.

3.2 Methodology

3.2.1 Total Energy Calculation

All self-consistent total energy calculations were based on the spin-polarized density functional theory (DFT) as implemented in the Quantum ESPRESSO simulation package[44, 45]. All-electron projected augmented wave (PAW) pseudopotentials were used to describe the electron-ion interactions[46, 47]. Generalized gradient approximation (GGA) in the framework of Perdew–Burke–Ernzerhof (PBE) used to evaluate electronic exchange-correlation interactions[48]. To consider the long-range dispersion forces, the semi-empirical van der Waals corrections DFT-D3 proposed by Grimme et. al were employed[49]. To avoid interaction between two periodic images, a vacuum of 15 Å was provided in **z**-direction. The kinetic energy cut-off for the plane-wave basis set was chosen to be 60 Ry. The convergence threshold for geometry optimization was set to 1.0×10^{-7} eV without applying any symmetry constraints. The Marzari-Vanderbilt smearing method with a finite temperature width of 0.02 Ry was adopted[50]. Supercells consisting of $2 \times 2 \times 1$ Ψ-graphene unit cell‘ were used and the Brillouin zones were sampled using a Monkhorst–Pack scheme with $7 \times 5 \times 1$ **k**-points grid[51].

3.2.2 Electronic Reactivity Descriptors (ERDs) calculation

The d-band centre (ϵ_d), d-band width (W_d) and fractional filling of d-band (f_l) are regarded as ERDs, which predicts the reactivity of transition-metal based catalyst based on the change in electronic structure of the catalyst are calculated as

$$\varepsilon_d = \frac{\int_{-\infty}^{E_F}(E-E_F)D_{d\sigma}(E)dE}{\int_{-\infty}^{E_F}D_{d\sigma}(E)dE} \quad ...(1)$$

$$W_d = \frac{\int_{-\infty}^{E_F}D_{d\sigma}(E)[(E-E_F)-\varepsilon_d]^2dE}{\int_{-\infty}^{E_F}D_{d\sigma}(E)dE} ...(2)$$

$$f_l = \frac{\int_{-\infty}^{E_F}D_{d\sigma}(E)dE}{\int_{-\infty}^{\infty}D_{d\sigma}(E)dE} ...(3)$$

Where $D_{d\sigma}(E)dE$ ($\sigma = \uparrow, \downarrow$) is the DOS projected on the d-states of Co atom, E is the energy and E_F is the Fermi energy of the system[52–54].

3.2.3 Activation Energy and Minimum Energy Path calculation

The minimum energy path (MEP), transition states (TSs) of CO oxidation reaction mechanism were investigated using the climbing image nudged elastic band (CI-NEB) method proposed by Henkelman et al. (implemented in the Quantum ESPRESSO)[55, 56]. Similar convergence criteria and computational parameters (including the PBE+D3 approach) were adopted for the investigation of reaction path, as considered for geometry relaxation. The activation energy barrier (E_a) for each reaction step was obtained using the following formula

$$E_a = E_{TS} - E_{IS/IM} ...(4)$$

Where E_{TS} and $E_{IS/IM}$ are the energies of transition state, initial/intermediate state (depend on the nature of reaction). In our study, XCrySDen visualization package was used to prepare all visual depictions of the structures under investigation[57].

3.3 Results and Discussion

3.3.1 Structural stability and electronic properties of Co@PG

The catalytic behaviour of a single atom catalyst heavily relies on its interaction with the substrate and has been investigated extensively in this study. Fig.3.2a shows the optimized geometry of 12 atoms unit cell of PG composed of 5-6-5 carbon rings. The optimized lattice parameters a= 6.70 Å and b= 4.84 Å are matching well with the previous reports. Owing to the structural asymmetry, total 14 inequivalent adsorption sites exists in the unit cell of PG, viz. six bridge sites (B1-B6), four hollow sites (H1-H4) and four top sites (T1-T4), as indicated in the Fig.3.2b[43]. In this investigation, 2 × 2 supercell of PG (containing 48 carbon atoms) is adopted which is sufficient for anchoring Co single atom. Beginning with, determination of the minimum energy site for Co over PG, all 14 sites were taken into account and the corresponding binding energy of Co@PG is obtained using

$$E_b = E_{Co@PG} - E_{PG} - E_{Co} ...(5)$$

Where $E_{Co@PG}$, is the total energy of Co@PG, E_{PG} is the total energy of clean PG sheet and E_{Co} is the energy of an isolated Co atom, respectively. The computed binding energy and average C-Co bond lengths of Co over PG for all considered sites are available in Table S1. The analysis suggests that Co prefers to sit on H4 site with higher binding energy 3.37 eV and relatively shorter average bond length of 2.04 Å between C-Co as shown in Fig.3.3a. In fact, during the complete geometry optimization of Co atom on sites like T2, T4, B1, B2, B3 over PG, end up on the H4 site, indicating its high affinity towards H4 site. Therefore, Co over H4 site of PG configuration (Co@PG) adopted as representative system to perform further calculations. To study the correlation between stability of structural geometry and electronic structure of the representative system analysis of partial density of states (PDOS) can provide valuable insight. In the PDOS of Co@PG system, presented in Fig.3.3b, shows the strong overlapping between 2p-orbital of C-atom and 4d-orbital of Co-atom, suggesting strong bonding between the Co-atom and substrate. The occurrence of sharp peaks in the proximity of fermi level indicative of high degree of chemical reactivity of Co@PG (as highlighted in the inset picture)[6, 36, 37]. Further looking into the electronic reactivity of Co@PG, the calculated values of d-band centre ($\epsilon_{d\uparrow}$ and $\epsilon_{d\downarrow}$) for spin-up and spin-down states of Co are -1.83 eV and -1.23 eV, respectively along with the values of fractional filling of d-band ($f_{l\uparrow}$ and $f_{l\downarrow}$) 0.94 and 0.68 indicates that the minority-spin state of Co would be interacting prominently with the reactants and intermediates. The asymmetric nature of PDOS plot of CO@PG in spin-up and spin-down state channels, hints at the magnetically active behaviour of the system[37]. Lowdin charge analysis confirms the considerable charge (0.73 e^-) transfer from Co-atom to the substrate, validating the concept of strong metal-support interaction orbital hybridization[39].

The mobility of single atom catalysts over substrate is a key kinetic parameter to examine its stability and durability. The dispersed atom should be highly immobile at ambient and also at extreme reaction conditions in order to have a stable and durable SAC. Thus, the diffusion pathway of Co atom over PG from H4 site to next nearest H4 site, was studied by employing CI-NEB method and depicted in Fig5.3. In order to diffuse from one H4 site to next nearest H4 site, Co has to overcome higher energy barrier of 3.18 eV. Moreover, using theory of absolute velocities, the diffusion rate (v) was computed using the formula[58]

$$\mathrm{v} = \nu \times exp(-E_a/K_BT)...(6)$$

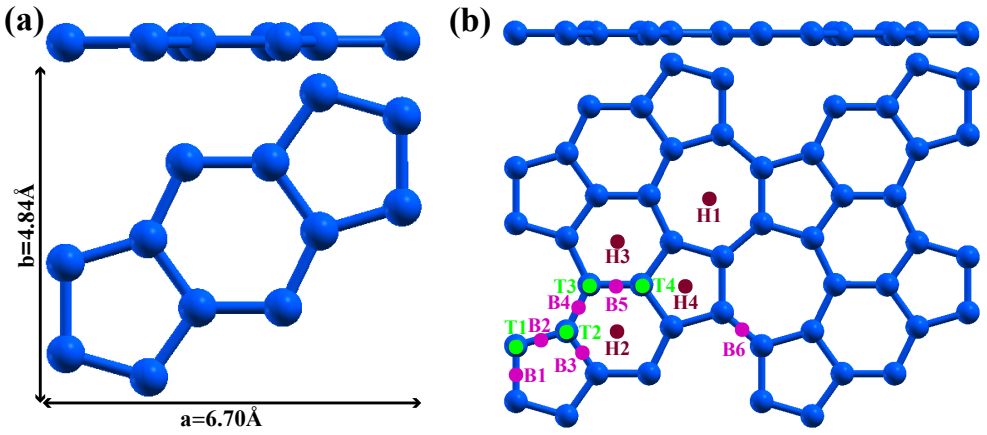

FIGURE 3.2: Side and Top view of (a) optimized geometry of PG unit cell with the optimized lattice parameters and (b) 2×2 super cell of PG with representation of possible anchoring site for single atom catalyst.

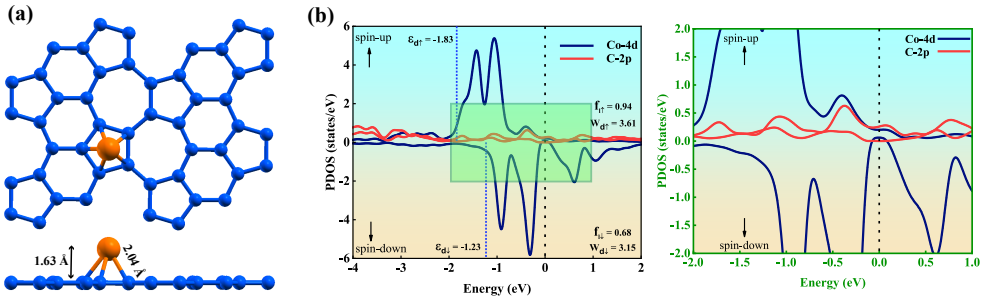

FIGURE 3.3: (a) Top and Side view of Co adsorbed over H4 site over PG (Co@PG). Blue and orange sphere represent C of PG and Co atoms, respectively (b) The plot of spin polarized partial density of states (PDOS) projected on Co-4d (dark blue) and C-2p (red) states of Co@PG system. The fermi level is set to zero. The corresponding ERDs data are presented in inset and the dashed light blue represent d-band centre for spin-up and spin-down states.

Where, ν is the vibrational frequency (taken as $\nu = 10^{13}s^{-1}$) , K_B is the Boltzmann constant and T is the absolute temperature and E_a is the diffusion barrier (3.18 eV)[59]. The estimated diffusion rate is found to be of the order of $10^{-41}s^{-1}$ at room temperature (300K) and $10^{-9}s^{-1}$ at 750K, which is far lower even at elevated temperature. Also, the lifetime (τ) of a Co atom over particular site (here H4), also regarded as residual time or time duration for Co staying on H4 site, is a parameter to estimate its dynamic behaviour and it can be obtained using Arrhenius equation as: $\tau = 1/\nu$, where v is the diffusion rate[58]. The calculated value of τ is of the order of 10^{35} days at room temperature and is nearly 2700 days at 750K accentuate the dynamic stability of Co single atom on the substrate even at ambient reaction conditions. Thus, rather high diffusion barrier, relatively lower diffusion rate and substantially high lifetime at room temperature

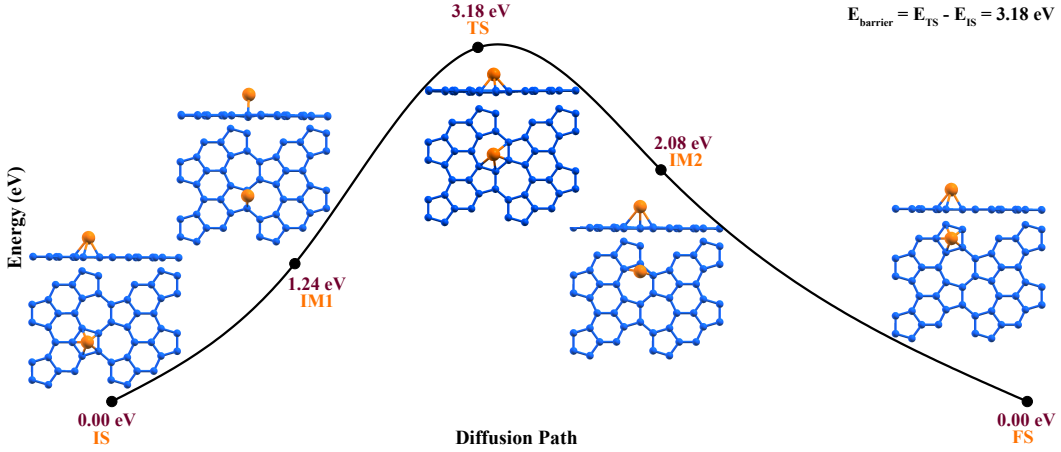

FIGURE 3.4: The diffusion pathway of Co atom from one H4 site to next nearest H4 site over PG.The corresponding diffusion barrier is 3.18 eV.

combinedly points at the lower mobility of isolated Co atoms on substrate and thus implying high kinetic stability of Co@PG.

'No cluster formation' of the dispersed metal atoms on the substrate is the indispensable condition specially in case of SACs. Quite oppositely, the transition metals (TM) have higher tendency to form clusters over substrate. Thus, Co dimerization have been examined by means of the energy difference (ΔE) between two Co atoms dispersed on two different H4 sites ($2Co_1$) and Co dimer adsorbed at a H4 site (Co_{dimer})[6]. The optimized geometry of two Co atoms dispersed on two different H4 sites and Co dimer adsorbed at a H4 site of PG is presented in Fig.3.5a and Fig.3.5b, respectively.

$$\Delta E = E_{(2Co_1)} - E_{(Co_{dimer})} ...(7)$$

Where, $E_{(2Co_1)}$ and $E_{(Co_{dimer})}$ are the energies of two Co atoms dispersed on two different H4 sites and Co dimer adsorbed at a H4 site. The computed value of ΔE confirms that dispersed Co atoms are favoured by 0.54 eV as compared to the dimers over PG. Factors such as strong binding energy, high diffusion barrier, lower diffusion rate impose the structural stability of the representative system Co@PG and high relative energy difference (ΔE) denies the possibility of cluster formation over substrate.

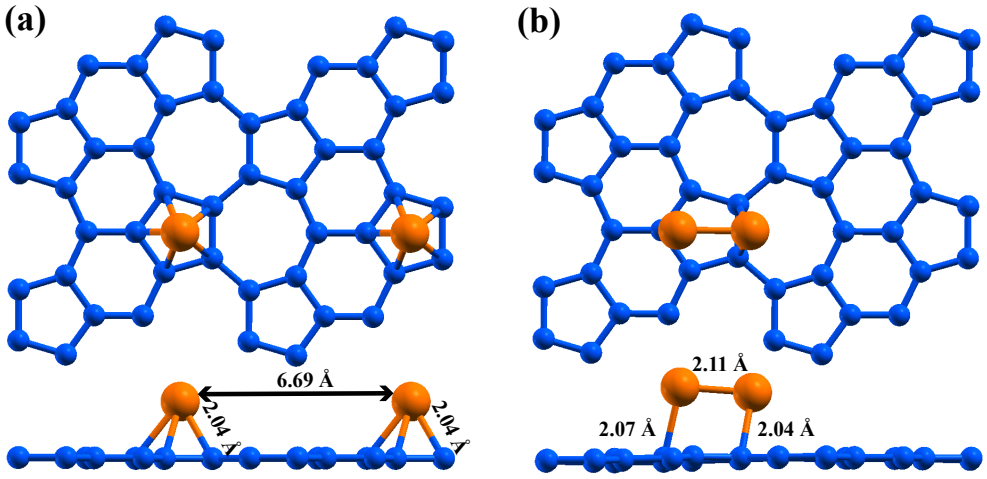

FIGURE 3.5: Top and Side view of (a) Two Co atoms adsorbed over two different H4 sites of PG (b)Co dimer adsorbed over a H4 site.

3.3.2 Adsorption of species over Co@PG

The performance of SACs is driven by how it interacts with the reactant species. For CO oxidation, it is of prime significance to understand the adsorption and activation of reactants such as CO/O_2 and Co@PG to gain fundamental insight of interaction mechanism over the catalyst. Thus, the individual and co-adsorption of reactants (CO and O_2) were carried out over Co@PG. The corresponding adsorption energies of reactants are calculated using following equation

$$E_{ads} = E_{molecule+Co@PG} - E_{Co@PG} - E_{molecule} ...(8)$$

where, $E_{molecule+Co@PG}$, $E_{Co@PG}$ and $E_{molecule}$ are the total energy of single/co-adsorbed molecule over Co@PG, energy of Co@PG and energy of isolated molecule. To study O_2 interaction mechanism over Co@PG, end-on (where O-O moiety points towards Co atom forming Co-O bond) and side-on (where O_2 molecules lies exactly parallel to the PG sheet) configurations were taken into consideration. The O_2 molecule prefers to bind with side-on configuration and its optimized geometry with structural parameters are presented in Fig.3.6a. It's relatively high adsorption energy of -2.96 eV complements to the significantly higher charge transfer (0.61 e^-) from Co@PG to O_2 molecule. The PDOS plot presented in Fig.3.6b of free (orange & pink thin lines for $O_{(1)}$ & $O_{(2)}$ respectively) and adsorbed (red & green thick lines for $O_{(1)}$ & $O_{(2)}$ respectively) O_2 molecule over Co@PG shows, after the adsorption of O_2 molecule, the peak of $O_{(1)}/O_{(2)}$-2p orbital shifts (near the Fermi level) such that there is a complete overlapping between $O_{(1)}/O_{(2)}$-2p

and Co-4d (blue thick line) orbitals, implying stronger interaction between Co and O_2 owing to the p-d hybridization. Moreover, the elongation of O-O bond length (d_{o-o} =1.38Å) compared to free O_2 molecule (1.23Å) indicates the activation of O_2 molecule over Co@PG, which is quite essential for CO oxidation reaction. Concisely, higher adsorption energy, significant charge transfer, strong overlapping of Co-4d and $O_{(1)}/O_{(2)}$-2p states and elongated O-O bond length signifies strong interaction and activation of O_2 over Co@PG system. Likewise, O_2 adsorption,

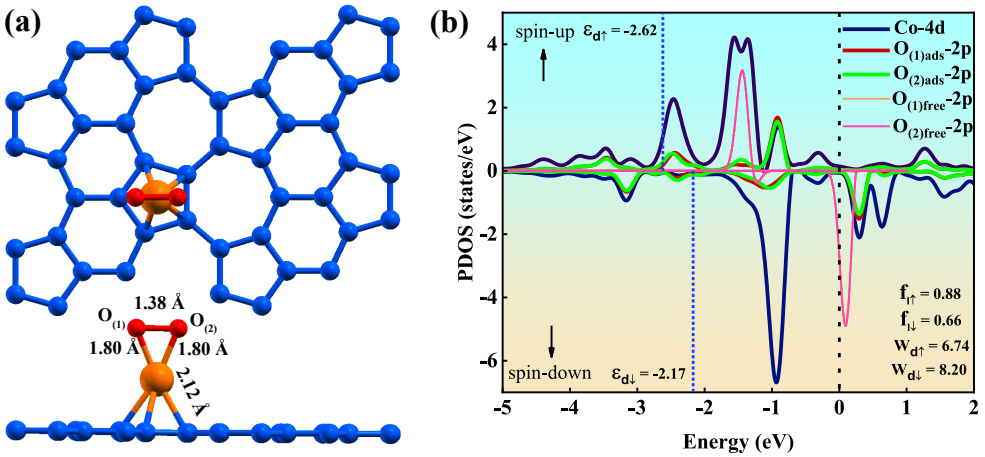

FIGURE 3.6: (a) Top and side views of most stable configuration of $O_2/Co@PG$. (b) spin polarized PDOS plot of $O_2/Co@PG$ along with calculated ERDs. The Fermi level is set to zero. Red sphere represents O atom.

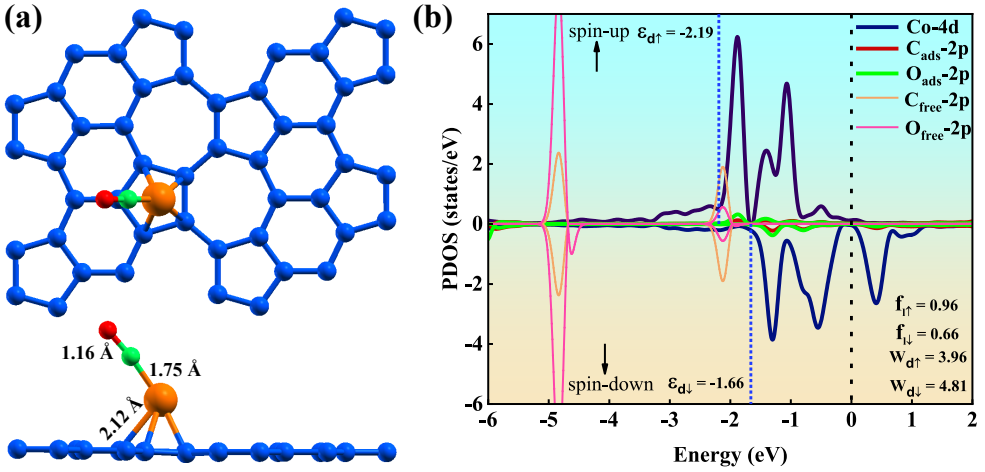

FIGURE 3.7: (a) Top and side views of most stable configuration of CO/Co@PG. (b) spin-polarized PDOS plot of CO/Co@PG along with calculated ERDs. The Fermi level is set to zero. Green sphere represents C atom of CO.

both side-on and end-on configurations were examined for CO adsorption over Co@PG with and turns out that CO prefers end-on configuration via forming Co-C bond of 1.75 Å as shown in Fig.3.7a. The CO adsorption energy is -2.58

eV, which is rather less exothermic compared to O_2 adsorption energy (-2.96 eV) recommending that the O_2 adsorption is more favoured by Co@PG. The PDOS plot of free (orange & pink thin lines for C & O respectively) and adsorbed (red & green thick lines for C & O respectively) CO over Co@PG is presented in Fig.3.7b. After CO adsorption, the C-2p & O-2p states of CO has significant overlapping with Co-4d states in the energy range of -2 to 1 eV which accounts for adequate CO adsorption that is benign for further CO oxidation process. Moreover, the C-O bond length (1.16 Å) is elongated by 0.02 Å compared to free CO molecule (1.14 Å) supporting the reasonable charge transfer (0.51 e^-) from Co@PG to CO molecule. Another critical geometrical parameter is the Co-C-O bond angle; the CO molecule binds in more of a linear fashion with ∠Co-C-O is found to be 174°. The linear structure of CO molecule illustrates notable back-donation of electrons from the metal centre to CO molecule which authenticate the results of decent CO adsorption energy. The mid-range CO adsorption energy, elongation in C-O bond and substantial charge transfer ascertain tepid binding of CO with Co@PG, which in turn is pivotal in reducing CO poisoning and thus certainly boost the catalyst performance.

The d-band centre of Co, initially at -1.83 eV ($\epsilon_{d\uparrow}$) and -1.23 eV ($\epsilon_{d\downarrow}$) after O_2 adsorption has been shifted by 0.79 eV($\epsilon_{d\uparrow}$=-2.62 eV) and 0.94 eV($\epsilon_{d\downarrow}$=-2.17 eV) away from Fermi level, while in the case of CO adsorption it has been shifted by 0.36 ($\epsilon_{d\uparrow}$=-2.19 eV) and 0.43 eV($\epsilon_{d\downarrow}$=-1.66 eV) away from Fermi level, as presented in Fig.3.6b and Fig.3.7b. It is safe to say that the relatively large shifts of $\epsilon_{d\uparrow}$ and $\epsilon_{d\downarrow}$ after O_2 adsorption as compared to CO adsorption indicate stronger interaction of O_2 than CO with Co@PG. Analysis of above results suggests that Co@PG is extremely proficient in O_2 activation, which is a key step in CO oxidation reaction.

The adsorption of atomic O and CO_2 molecule over Co@PG has also been examined. As shown in Fig.3.8a O adatom binds to Co with relatively shorter bond length of 1.60 Å as compared to O_2 molecule (1.80 Å) hinting at a strong interaction of O adatom with Co and confirmed by elevated O adsorption energy of -5.62 eV. Also, higher amount of charge transfer (0.93 e^-) occurring from Co@PG to O justifies the strong interaction of O atom with Co@PG. The study of CO_2 interaction with the catalyst is vital in order to understand whether the system is competent enough to avoid CO_2 poisoning. Typically, the CO_2 molecule should not interact too strongly and its interaction energy should not be higher than 0.5 eV with the catalyst with the aim that CO_2 should be set free at once as a product of the reaction[60]. As depicted in Fig.3.8b, CO_2 molecule is physiosorbed and lies

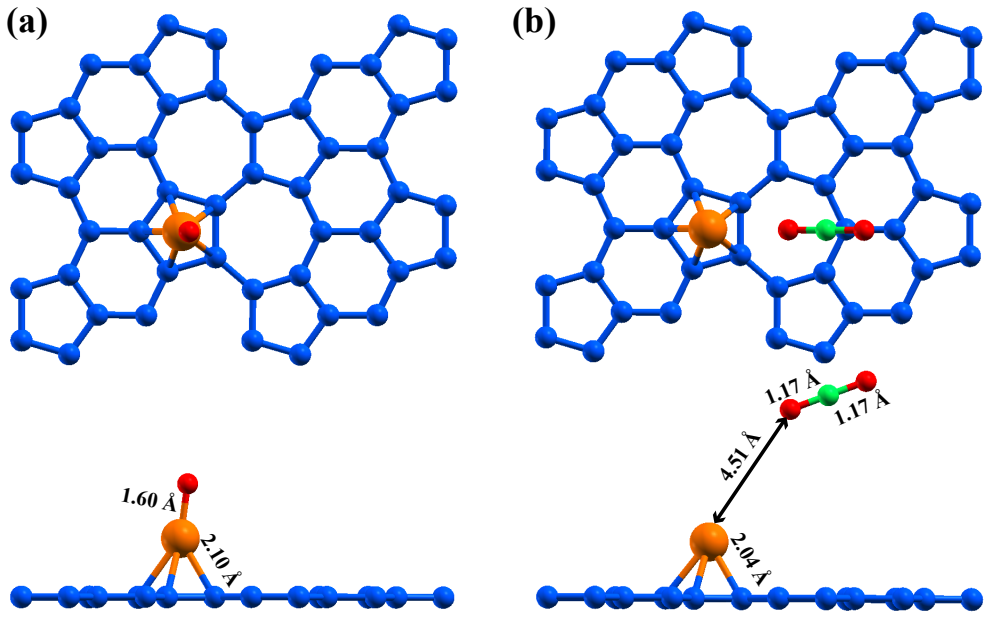

FIGURE 3.8: Top and side views of most stable configuration of (a) O adatom and (b) CO_2 in the gas phase over Co@PG.

well above the Co@PG with C-O bond length of 1.17 Å, that is unaltered with respect to free CO_2 molecule. The interaction energy of CO_2 molecule over Co@PG is found to be as low as 0.056 eV thereby signifying its potential in avoiding CO_2 poisoning and readily releasing CO_2.

Secondly, the capture-performance (co-adsorption of reactants) over the catalyst has been investigated as it is of great significance in deciding the possible reaction mechanism. The optimized geometry of co-adsorbed reactants on Co@PG, i.e., CO+O_2 and CO+CO are presented in Fig.3.9(a-b). The co-adsorption energy of CO+O_2 (-4.91 eV) and CO+CO (-4.63 eV) is markedly higher than that of adsorption energies of individually adsorbed CO (-2.58 eV) and O_2 (-2.96 eV) which implies that the Co@PG can anchor two reactants comprehensively. In addition, the large value of co-adsorption energies and the small difference in adsorption energy of individual CO and O_2 promote the catalytic CO oxidation reaction and aid in deciding a particular reaction mechanism for CO oxidation process.

In accordance with the above discussion of individual and co-adsorption energy of CO, O_2, 2CO and CO+O_2, the feasibility of CO+O_2 co-adsorption directly implies that there is all likelihood that CO oxidation reaction might follow LH mechanism in which both the reactants are co-adsorbed over the catalyst surface. Additionally, Co SAC adsorbs and activate O_2 molecule proficiently compared to CO molecule, there is a high odds of CO oxidation reaction following ER mechanism in which the reactant having lower adsorption energy (here CO) approach

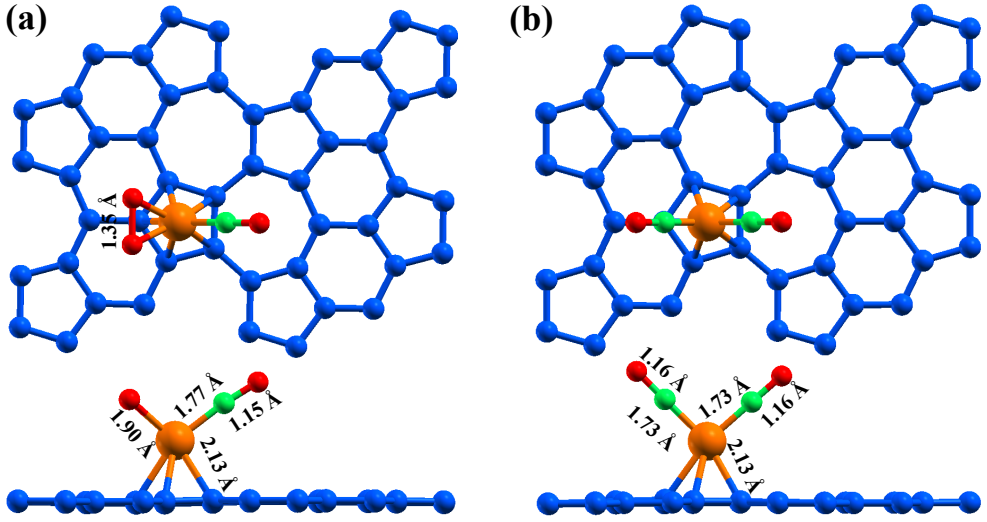

FIGURE 3.9: Top and side views of most stable configuration of (a) CO+O_2/Co@PG and (b) CO+CO/Co@PG.

to interact with another already adsorbed and activated reactant with high adsorption energy (here O_2). Hence, here we studied both, LH and ER mechanism of CO oxidation reaction over Co@PG SAC[61, 62].

3.3.3 CO oxidation over Co/PG

3.3.3.1 LH Mechanism

The capability of hosting both reactants simultaneously is prerequisite condition for LH mechanism of CO oxidation. Thus, LH mechanism of CO oxidation over the Co@PG have been considered first to be investigated in this study. To begin with, we considered the sum of total energies of Co@PG, two isloted CO molecules, isolated O_2 molecule as the reference to compare and compute the energies of each elementary reaction steps and activation barriers. In the first half of LH mechanism (LH1), the initial state (IS-LH1) is comprised of co-adsorbed CO-O_2 molecules over CO@PG. The whole reaction pathway and activation barriers for sequential steps are depicted in Fig.3.10. As depicted in the Fig.3.10, in the IS-LH1 itself, the O_2 molecule gets activated which is confirmed by the elongation of O-O bond by 0.12Å (1.35Å) as compared to free O_2 molecule (1.23Å). This means that catalyst is certainly effective to activate and break O-O bond which is the foremost requirement in the formation of first CO_2 molecule during CO oxidation reaction. Further, the C atom of CO molecule advances towards the O_2

molecule with activation barrier of 0.05 eV only to form the transition state (TS-LH1), where the O-O bond further elongates to 1.38Å, activating O_2 molecule. As the CO and O_2 molecule reacts, there is a highly exothermic OCOO* complex formation taking place releasing 2.81 eV, thereby forming an intermediate state (IM-LH1) which is referred as triangular reaction intermediate (TRI). Here, the TRI formation is troublesome step due to its higher stablility. Next, the higher barrier of 1.05 eV is required for the OCOO* dissociation and release of first CO_2 molecule thereby achieving the final state (FS-LH1). This first half reaction, is exothermic process with reaction energy of 1.71 eV. However, this reaction is thermodynamically favourable but kinetically its challenging and not feasible as the second barrier is relatively high, indicating at the inefficiency of Co@PG to release CO_2 molecule. This is attributed to the stronger co-adsorption of CO and O_2 and intermediates with the Co@PG, making it difficult to release the product.

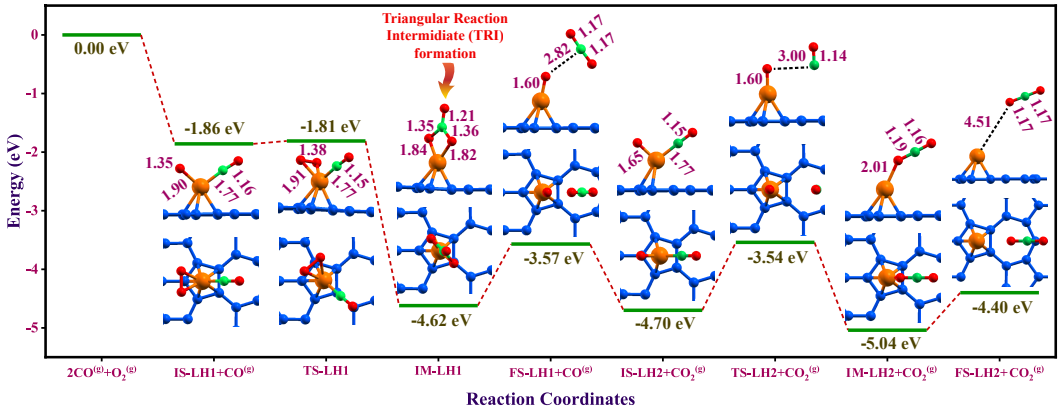

FIGURE 3.10: The minimum energy pathway and geometric configurations of different states like IS, IM, TS and FS for CO oxidation reaction via LH mechanism on Co@PG. Hereafter, IS, IM, TS and FS represents initial, intermediate, transition and final states of the reaction.The corresponding bond lengths (in Å) between various species are mentioned in respective images.

Further, in the second half of the LH reaction mechanism (LH2), the single activated O-atom reacts with second CO and oxidise to CO_2. As shown in Fig.3.10 (IS-LH2), the O-atom left from the previous step and adsorbed CO molecule reacts on the catalytic centre forming a linear OCO molecule (IM-LH2) via TS-LH2 with relatively higher activation barrier of 1.16 eV. Further the OCO complex is released forming physiosorbed CO_2 molecule as in FS-LH2 with step barrier of 0.64eV. Thus, the second half of CO oxidation is also impractical owing to high activation energy of 1.16eV and higher endothermicity in releasing the product

CO_2. From the above discussion, it is safe to say that CO oxidation via LH mechanism is idle over Co@PG. So, the study proceeds for determining and analysing alternate reaction mechanism.

3.3.3.2 ER Mechanism

The CO oxidation process through ER mechanism in which one of the reactants (primarily O_2) is pre-adsorbed at the catalytically active site and interact with the other reactant (CO) form the gas phase and forms the product. As Co@PG have stronger interaction with O_2 compared to CO, the probability of CO poisoning over the catalyst can be avoided as the catalytic centre will not be directly exposed to the CO, thereby improves the durability of the catalyst. Fig.3.11 shows complete reaction pathway of the CO oxidation via ER mechanism where in the first half reaction (ER1), the initial state (IS-ER1) comprising of O_2 molecule being activated by occupying the catalytic site and CO (physiosorbed) lies far away at 3.52Å from nearest O-atom. As the reaction proceed, the C-atom of CO approaches the nearest O-atom of O_2 (IM1-ER1). The O-O bond breaks forming O-C-O complex in the TS-ER1 with activation barrier of 0.19 eV and releasing CO_2 as product (FS-ER1). The first-half reaction of CO_2 formation is highly exothermic step releasing about 2.76 eV energy indicates that CO_2 molecule can be emitted swiftly. Thus, the formation of first CO_2 molecule is thermodynamically and kinetically favourable.

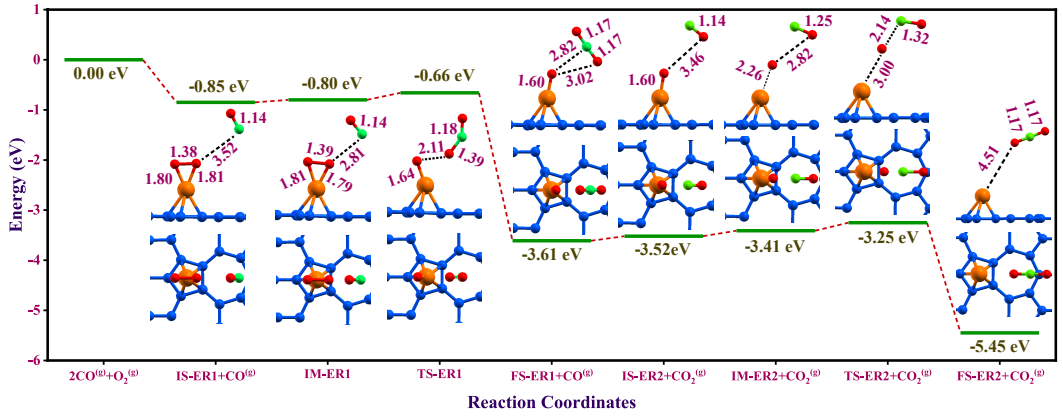

FIGURE 3.11: The minimum energy pathway and geometric configurations of different states like IS, IM, TS and FS for first half CO oxidation reaction via ER mechanism on Co@PG.

Subsequently, the O atom left from first-half CO oxidation reaction would be further interacting with another CO atom in second-half reaction (ER2) as $CO^{(g)}$

TABLE 3.1: The Co-atom binding energy (E_b(Co)),adsorption energy of CO ($E_{ads}(CO)$) & O_2 ($E_{ads}(O_2)$) molecule and activation energy (E_a) corresponding to 1^{st} & 2^{nd} half of CO oxidation reaction (preferable reaction mechanism mentioned in superscript) over Co SAC on various substrates.

Catalyst	E_b(Co) (eV)	$E_{ads}(O_2)$ (eV)	$E_{ads}(CO)$ (eV)	E_a $(eV)^{mechanism}$ $1^{st}/2^{nd}$
Co@PG (our work)	-3.37	-2.96	-2.58	$0.19^{ER}/0.27^{ER}$
Co/SV-Gra[65]	-8.51	-1.75	-0.62	$0.42^{LH}/0.19^{ER}$
Co/Graphenylene[67]	-2.74	-2.64	-2.05	$0.38^{LH}/0.11^{LH}$
Co/DV-Gra[64]	-7.39	-1.61	-1.32	$0.31^{LH}/0.36^{LH}$
Co/N3-Gra[63]	-7.61	-1.95	-0.65	$0.87^{ER}/0.20^{ER}$
Co/g-C3N4[6]	-3.25	-2.12	-1.74	$0.16^{TER}/0.21^{TER}$ $0.25^{ER}/0.40^{ER}$
Co/SV-Gra[66]	-8.51	-1.75	-0.62	$0.28^{LH}/0.38^{ER}$
Co/VB-hBN[35]	-8.64	-1.41	-1.15	$0.52^{ER}/0.32^{ER}$
Co/VB-hBN[68]	-8.81	-0.88	-1.04	$0.17^{LH}/0.55^{LH}$

$+O^* \rightarrow CO_2^{(g)}$. As shown in Fig.3.11, IS-ER2 consists of pre-adsorbed O-atom with CO in gas phase and further CO molecule is approaching O atom and breaking Co-O bond to form TS-ER2 via IM-ER2 state with activation barrier of 0.27 eV. Further, the reaction process is highly exothermic releasing around 2 eV energy by forming second CO_2 molecule (FS-ER2) in the gas phase. The formation of second CO_2 molecule on Co@PG via ER mechanism is practicable with lower activation energy and exothermicity of the reaction process. Thence, Co@PG is comprehensively competent for CO oxidation reaction via ER mechanism.

To emphasize on the exceptional catalytic performance of Co@PG, we compared our results with previous reported studies on Co SAC over various substrates for CO oxidation reaction. As summerized in Table 3.1, the Co@PG via ER mechanism exhibit remarkably lower activation barrier (0.19 eV/0.27 eV) as compared to Co SAC on other substrates like graphene[63–66], graphenylene[67] & h-BN[35, 68] which ranges from 0.31 eV to 0.87 eV. Thus, Co@PG holds great promise to be a cogent next-gen catalyst towards CO oxidation reaction.

3.4 Conclusion

In this study, the potential of Ψ-graphene supported Co single atom catalyst (Co@PG) for electrocatalytic CO oxidation reaction has been meticulously examined by means of spin-polarized, dispersion corrected DFT calculations. With

the quite high diffusion barrier, extremely lower diffusion rate and relative energy difference brings out the stoned-stability and foreclose the possibility of cluster formation of Co atom over substrate, thereby improving the usage durability of Co@PG. Further, the calculated adsorption/co-adsorption energy and plots of spin-polarized PDOS of reactants (CO, O_2) over Co@PG corroborates that the catalyst is accomplished to capture and activate the reactants comprehensively. The LH and ER mechanisms have been performed over Co@PG for CO oxidation. The Co@PG shows exquisite catalytic behaviour with lower activation barrier of 0.19 eV and 0.27 eV for first and second half of CO oxidation reaction via ER mechanism. Consequently, our study exhaustively presents a computational way of designing a rational catalyst for electrocatalytic CO oxidation reaction and also offers practicable insights for developing a non-noble, economically efficient and potent catalyst for experimentation.

Bibliography

[1] S. K. Kaiser, Z. Chen, D. Faust Akl *et al.* *Chemical reviews*, 120(21):11703–11809, 2020.

[2] H. Zhang, S. Fang and Y. H. Hu. *Catalysis Reviews*, 64(3):491–532, 2022.

[3] Q. Jiang, J. Zhang, Z. Ao *et al.* *Frontiers in chemistry*, 6:187, 2018.

[4] L. Nie, D. Mei, H. Xiong *et al.* *Science*, 358(6369):1419–1423, 2017.

[5] X.-Q. Gong, Z.-P. Liu, R. Raval *et al.* *Journal of the American Chemical Society*, 126(1):8–9, 2004.

[6] S. Wang, J. Li, Q. Li *et al.* *Nanoscale*, 12(1):364–371, 2020.

[7] Y. Lou, Y. Cai, W. Hu *et al.* *ACS Catalysis*, 10(11):6094–6101, 2020.

[8] J.-C. Liu, Y.-G. Wang and J. Li. *Journal of the American Chemical Society*, 139(17):6190–6199, 2017.

[9] C. Jia, X. Wang, H. Yin *et al.* *Journal of Materials Chemistry A*, 9(4):2093–2098, 2021.

[10] Y. Tang, H. Zhang, J. Zhou *et al.* *New Journal of Chemistry*, 43(24):9555–9565, 2019.

[11] Q. Liu and Z. Zhang. *Catalysis Science & Technology*, 9(18):4821–4834, 2019.

[12] X. Liu, M. Xu, L. Wan *et al.* *ACS Catalysis*, 10(5):3084–3093, 2020.

[13] E. J. Peterson, A. T. DeLaRiva, S. Lin *et al.* *Nature communications*, 5(1):4885, 2014.

[14] G. Spezzati, Y. Su, J. P. Hofmann *et al.* *Acs Catalysis*, 7(10):6887–6891, 2017.

[15] Y. Tang, J. Zhou, Z. Shen *et al. RSC advances*, 6(96):93985–93996, 2016.

[16] Y. Li, Z. Zhou, G. Yu *et al. The Journal of Physical Chemistry C*, 114(14):6250–6254, 2010.

[17] E. Song, Z. Wen and Q. Jiang. *The Journal of Physical Chemistry C*, 115(9):3678–3683, 2011.

[18] X.-Y. Xu, J. Li, H. Xu *et al. New Journal of Chemistry*, 40(11):9361–9369, 2016.

[19] Z. Fu, B. Yang and R. Wu. *Physical review letters*, 125(15):156001, 2020.

[20] Z. Chen, L. Chen, C. Yang *et al. Journal of Materials Chemistry A*, 7(8):3492–3515, 2019.

[21] F. Li, Y. Li, X. C. Zeng *et al. Acs Catalysis*, 5(2):544–552, 2015.

[22] L. Liu and A. Corma. *Chemical reviews*, 118(10):4981–5079, 2018.

[23] B. Qiao, A. Wang, X. Yang *et al. Nature chemistry*, 3(8):634–641, 2011.

[24] Y. Feng, Q. Wan, H. Xiong *et al. The Journal of Physical Chemistry C*, 122(39):22460–22468, 2018.

[25] Z. Lu, P. Lv, J. Xue *et al. RSC advances*, 5(103):84381–84388, 2015.

[26] Q. Jiang, J. Zhang, H. Huang *et al. Journal of Materials Chemistry A*, 8(1):287–295, 2020.

[27] J.-X. Liang, X.-F. Yang, A. Wang *et al. Catalysis Science & Technology*, 6(18):6886–6892, 2016.

[28] L. Qin, Y.-Q. Cui, T.-L. Deng *et al. ChemPhysChem*, 19(24):3346–3349, 2018.

[29] J.-X. Liang, J. Lin, X.-F. Yang *et al. The Journal of Physical Chemistry C*, 118(38):21945–21951, 2014.

[30] P. Wu, P. Du, H. Zhang *et al. Physical Chemistry Chemical Physics*, 17(2):1441–1449, 2015.

[31] K. Mao, L. Li, W. Zhang *et al. Scientific reports*, 4(1):5441, 2014.

[32] J. Liang, Q. Yu, X. Yang *et al. Nano Research*, 11:1599–1611, 2018.

[33] T. Yang, R. Fukuda, S. Hosokawa *et al.* *ChemCatChem*, 9(7):1222–1229, 2017.

[34] H. Xu, C.-Q. Xu, D. Cheng *et al.* *Catalysis Science & Technology*, 7(24):5860–5871, 2017.

[35] S. Lin, X. Ye, R. S. Johnson *et al.* *The Journal of Physical Chemistry C*, 117(33):17319–17326, 2013.

[36] Y.-C. Rao and X.-M. Duan. *Physical Chemistry Chemical Physics*, 21(46):25743–25748, 2019.

[37] S. Karmakar, C. Chowdhury and A. Datta. *The Journal of Physical Chemistry C*, 122(26):14488–14498, 2018.

[38] A. Wang, J. Li and T. Zhang. *Nature Reviews Chemistry*, 2(6):65–81, 2018.

[39] S. Tauster, S. Fung and R. L. Garten. *Journal of the American Chemical Society*, 100(1):170–175, 1978.

[40] L. C. Grabow, B. Hvolbæk and J. K. Nørskov. *Topics in Catalysis*, 53:298–310, 2010.

[41] M. B. Gawande, P. Fornasiero and R. Zboril. *Acs Catalysis*, 10(3):2231–2259, 2020.

[42] H. Fei, J. Dong, D. Chen *et al.* *Chemical Society Reviews*, 48(20):5207–5241, 2019.

[43] X. Li, Q. Wang and P. Jena. *The journal of physical chemistry letters*, 8(14):3234–3241, 2017.

[44] P. Giannozzi, S. Baroni, N. Bonini *et al.* *Journal of physics: Condensed matter*, 21(39):395502, 2009.

[45] P. Giannozzi, O. Andreussi, T. Brumme *et al.* *Journal of physics: Condensed matter*, 29(46):465901, 2017.

[46] P. E. Blöchl. *Physical review B*, 50(24):17953, 1994.

[47] G. Kresse and D. Joubert. *Physical review b*, 59(3):1758, 1999.

[48] J. P. Perdew, K. Burke and M. Ernzerhof. *Physical review letters*, 77(18):3865, 1996.

[49] S. Grimme, J. Antony, S. Ehrlich *et al.* *The Journal of chemical physics*, 132(15):154104, 2010.

[50] N. Marzari, D. Vanderbilt, A. De Vita *et al.* *Physical review letters*, 82(16):3296, 1999.

[51] H. J. Monkhorst and J. D. Pack. *Physical review B*, 13(12):5188, 1976.

[52] B. Hammer and J. K. Nørskov. In *Advances in catalysis*, volume 45, pages 71–129. Elsevier, 2000.

[53] S. Bhattacharjee, U. V. Waghmare and S.-C. Lee. *Scientific reports*, 6(1):1–10, 2016.

[54] B. A. Baraiya, H. Tanna, V. Mankad *et al.* *The Journal of Physical Chemistry A*, 125(24):5256–5272, 2021.

[55] G. Henkelman and H. Jónsson. *The Journal of chemical physics*, 113(22):9978–9985, 2000.

[56] G. Henkelman, B. P. Uberuaga and H. Jónsson. *The Journal of chemical physics*, 113(22):9901–9904, 2000.

[57] A. Kokalj. *Journal of Molecular Graphics and Modelling*, 17(3-4):176–179, 1999.

[58] Z. Lu, P. Lv, Z. Yang *et al.* *Physical Chemistry Chemical Physics*, 19(25):16795–16805, 2017.

[59] E. d. V. Gómez, S. Amaya-Roncancio, L. B. Avalle *et al.* *Applied Surface Science*, 420:1–8, 2017.

[60] B. He, J. Shen and Z. Tian. *Physical Chemistry Chemical Physics*, 18(35):24261–24269, 2016.

[61] Y.-H. Lu, M. Zhou, C. Zhang *et al.* *The Journal of Physical Chemistry C*, 113(47):20156–20160, 2009.

[62] Y. Li, Z. Zhou, G. Yu *et al.* *The Journal of Physical Chemistry C*, 114(14):6250–6254, 2010.

[63] Y. Tang, W. Chen, H. Chai *et al.* *The Journal of Physical Chemistry C*, 123(17):10926–10939, 2019.

[64] Y. Tang, W. Chen, Z. Shen *et al.* *Physical Chemistry Chemical Physics*, 20(4):2284–2295, 2018.

[65] Y. Tang, D. Ma, W. Chen *et al.* *Sensors and Actuators B: Chemical*, 211:227–234, 2015.

[66] Y. Tang, X. Dai, Z. Yang *et al.* *Carbon*, 71:139–149, 2014.

[67] Y. Tang, W. Chen, H. Zhang *et al.* *Physical Chemistry Chemical Physics*, 22(28):16224–16235, 2020.

[68] Z. Lu, P. Lv, Y. Liang *et al.* *Physical Chemistry Chemical Physics*, 18(31):21865–21870, 2016.